Microchimica Acta (2022) 189:392
https://doi.org/10.1007/s00604-022-05480-6

ORIGINAL PAPER

Colorimetric biosensor for visual determination of Golgi protein 73 based on reduced graphene oxide-carboxymethyl chitosan-Hemin/platinum@palladium nanozyme with peroxidase-like activity

Xinhao Li[1] · Shengnan Li[1] · Qiuyan Lv[1] · Chaoxian Wang[2] · Jintao Liang[1] · Zhide Zhou[1] · Guiyin Li[1,2]

Received: 1 July 2022 / Accepted: 26 August 2022 / Published online: 23 September 2022

Abstract

A Golgi protein 73 (GP73) colorimetric biosensor based on the reduced graphene oxide-carboxymethyl chitosan-hemin/platinum@palladium nanoparticles (RGO-CMCS-Hemin/Pt@Pd NPs) with peroxidase-like activity was constructed. The RGO-CMCS-Hemin/Pt@Pd NPs with high peroxidase-like activity were successfully synthesized under mild conditions. Then, the aminylated GP73 aptamer (Apt) was bound to the RGO-CMCS-Hemin/Pt@Pd NPs to form the recognition probe. Another unmodified GP73 aptamer (AptI) was served as the capture probe. In the presence of target GP73, the capture probe and the recognition probe specifically bind to GP73 and form a RGO-CMCS-Hemin/Pt@Pd NP-Apt/GP73/AptI sandwich-type structure, which can oxidase the colorless 3,3′,5,5′-tetramethylbenzidine (TMB) into blue oxTMB in the presence of H_2O_2. GP73 detection was achieved by measuring the peak UV absorption at 652 nm. Under the optimum conditions, the GP73 concentration was linearly related to the absorbance intensity in the range 10.0–110.0 ng/mL, and the limit of detection (LOD) was 4.7 ng/mL. The proposed colorimetric biosensor was successfully applied to detect GP73 in spiked human serum samples with recoveries of 98.2–107.0% and RSDs of 1.90–5.44%, demonstrating the excellent potential for highly sensitive GP73 detection in clinical detection.

Keywords Golgi protein 73 · RGO-CMCS-hemin/Pt@Pd NP nanozyme · Aptamer · Colorimetric sensor · Peroxidase-like activity

Introduction

Hepatic cell carcinoma (HCC) is one of the most common malignancies and is the second leading cause of tumor-related death [1]. Golgi glycoprotein 73 (GP73) is known as the Golgi membrane protein with a relative molecular weight of 73.104 kDa [2]. Elevated GP73 levels in cirrhosis, HCC, liver B, and acute chronic liver failure are closely associated with tumor metastasis, and serum GP73 expression levels in HCC patients promote the invasion and metastasis of HCC [3]. Therefore, GP73 becomes an ideal serum marker for the early diagnosis and postoperative recurrence of HCC. Meanwhile, GP73 can be used as an index of efficacy judgment after catheter arterial chemoembolization in primary HCC patients and has more advantages than alpha-fetal protein (AFP) [4]. Thus, it is excellently important to develop efficient, convenient, and inexpensive sensors to detect GP73 in clinic. At present, the detection of GP73 is based chiefly on immunoassay, which has high specificity and sensitivity. Yue Lin et al. [5] achieved the determination of GP73 by the

Highlights
- The RGO-CMCS-Hemin/Pt@Pd NPs with admirable peroxidase-like activity were synthesized.
- GP73 colorimetric sensor based on RGO-CMCS-Hemin/Pt@Pd NPs and aptamer was constructed.
- GP73 detection is achieved by measuring the absorbance changes for TMB-H_2O_2 system.
- GP73 biosensor responses linearly from 10.0 to 110.0 ng/mL with LOD of 4.7 ng/mL.
- GP73 colorimetric biosensor shows acceptable specificity and good recovery.

✉ Jintao Liang
dxljt@guet.edu.cn

✉ Zhide Zhou
zhouzhide10@guet.edu.cn

✉ Guiyin Li
liguiyin01@gdupt.edu.cn

Extended author information available on the last page of the article

specific binding of antigen and antibody with the minimum detection limit of 15 pg/mL. However, immunoassay relies on anti-GP73 antibodies, relatively expensive antibodies, complex instrumentation, and relatively stringent storage conditions, which make these methods costly.

Aptamer is a single-stranded oligonucleotide obtained from a DNA library of random sequences by in vitro selection technology [6] and is capable of recognizing various targets with high specificity and binding capacity. Compared with antibody, the aptamer is characterized by high specificity, high affinity, thermal stability, ease modification, low cost, and capacity to bind various molecules [7–9]. As far as GP73 aptamers are concerned, Jingchun Du et al. have screened specific GP73 aptamers by SELEX technique; the synthesized aptamer has high specificity and binding ability and can be used for clinical testing of GP73 [10]. Aptamer sensor (i.e., aptasensor), especially colorimetric aptasensor, has drawn much attention due to low cost, simplicity, and real-time detection without any special instruments, only using a UV–vis spectrophotometer or even the naked eye [11]. Recently, our group constructed a colorimetric sensor for the detection of GP73 with a detection limit of 5.41 ng/mL by coupling the aptamer to the reduced graphene oxide-trimanganese tetroxide (RGO-Mn_3O_4) nanoparticles [12]. Nevertheless, there is still a need to develop novel colorimetric aptasensors through the use of nanomaterials or nanomaterial-based nanozymes, which can be effective in catalyzing substrates to form significant color changes.

Nanozymes, nanomaterials with enzyme-like characteristics, are superior to natural enzymes for reason that they are typically constructed using inexpensive and mass-production methods and provide high operability, stability, and strong catalysis performance. Nanozymes include metal oxide-, metal-, and carbon-based nanozymes. according to their composition. Among them, Pt and Pd metal ions with peroxidase-like properties have catalytic activity for H_2O_2 decomposition [13, 14], and the catalytic activity of Pt@Pd nanoparticles are further enhanced by the interaction between them [15]. Moreover, hemin, a natural metal porphyrin, has the active center of redox proteins (such as hemoglobin, myoglobin, and peroxidase) [16]. Hemin is best characterized by peroxidase-like activity, where the substrates are TMB and H_2O_2; it can catalyze H_2O_2, so that the substrate is oxidized to produce different color products due to different electron loss conditions [17]. However, the molecular aggregation of hemin itself could reduce its catalytic activity; therefore, Hemin need be combined with a support material with a large specific surface area in order to achieve its stability and activity [18]. Reduced graphene oxide (RGO) demonstrates a large surface area, remarkable electrical conductivity, and high mechanical properties; Hemin can be firmly attached to RGO surface through van der Waals force and π-π bond interactions. The addition of RGO to Hemin can not only provide Hemin catalytic activity but also prevent Hemin and graphene aggregation [19]. Carboxymethyl chitosan (CMCS) is a chitosan derivative with good immunity, antibacterial and biodegradation, which is widely popular in biomedical care, environmental protection, food processing, and other applications [20].

In light of above considerations, we sought to develop a facile colorimetric aptasensor for GP73 detection based on the peroxidase-like activity of the reduced graphene oxide-carboxymethyl chitosan-Hemin/platinum@palladium nanoparticles (RGO-CMCS-Hemin/Pt@Pd NPs). The excellent peroxidase-like activity of the RGO-CMCS-Hemin/Pt@Pd NP nanozyme was verified by the 3,3′,5,5′-tetramethylbenzidine (TMB)-H_2O_2 system and the o-phenylenediamine (OPD)-H_2O_2 system. Next, the aminated GP73 aptamer (Apt) was bound to RGO-CMCS-Hemin/Pt@Pd NPs as the recognition nanoprobe. When the target GP73 is presence, the capture probe (an unmodified GP73 aptamer (AptI)) and recognition probe are specifically combined with GP73 and form an RGO-CMCS-Hemin/Pt@Pd NP-Apt/GP73/AptI sandwich-type structure. Taking advantage of the good peroxidase-like properties, RGO-CMCS-Hemin/Pt@Pd NPs can oxidase colorless TMB into blue oxTMB with the presence of H_2O_2; the absorbance of the system at 652 nm changed consequently, which realize the sensitive colorimetric detection of GP73. The RGO-CMCS-Hemin/Pt@Pd NP-based colorimetric aptasensor was used for sensitive and selective detection of GP73 in human serum samples.

Materials and methods

Chemicals and reagents

Golgi protein 73 (GP73), aminated GP73 aptamer (Apt,5′-NH_2-C6-GCAGTTGATCCTTTGGATACCCTGG-3′ [21]), another GP73 aptamer (AptI,5′-ACGCTCGGATGCCAC TACAGTTGGTTTTTTTTTGTTATTTAGAGTAAAAAC CTTGTGTGTAGTGACTCATGGACGTGCTGGTGAC-3′ [10]), and alpha fetal protein (AFP) were obtained from Sangon Biotech Co., Ltd. (Shanghai, China). Hemin, carboxymethyl chitosan (CMCS), Na_2PtCl_6, Na_2PdCl_6, immunoglobulin G (IgG), human serum albumin (HSA), bovine serum albumin (BSA), 3,3′,5,5′-tetramethylbenzidine (TMB), o-phenylenediamine (OPD), N-Hydroxysuccinimide (NHS), and 1-(3-Dimethylaminopropyl)-3-ethylcarbodiimide hydrochloride (EDC) were obtained from Aladdin Reagent Co., Ltd. (Shanghai, China). Ascorbic acid (AA), hydrazine hydrate, ammonium hydroxide, and H_2O_2 were obtained from Xilong Science Co., Ltd. (Guangdong, China). Single layer graphene oxide (GO) was obtained from Xianfeng Nanomaterials Technology Co., Ltd. (Nanjing, China). All chemicals were used without further purification, and all of

the experiments were performed using high-purity deionized water (18.25 MΩ·cm).

Apparatus and measurements

Scanning electron microscopy (SEM, SU8020) and transmission electron microscopy (TEM, G2 F30 S-TWIN) were employed to characterize the morphology and microstructures of the samples, respectively. Ultraviolet–visible (UV–vis) spectroscopy was recorded on a UH-5300 spectrophotometer (UV–vis, Hitachi, Japan). Elemental compositions are determined by Fourier transform infrared spectroscopy (FT-IR, Bruker Tensor 27, Germany), X-ray photoelectron spectroscopy (XPS, ESCALAB250Xi, Thermo-Fisher, USA), and *Raman* spectra (Raman, Renishaw inVia, England).

Preparation of the RGO-CMCS-Hemin/Pt@Pd NPs

First, the RGO-Hemin nanocomposites were produced according to the method of Li G et al. [22] (details in Electronic Supplementary Material (ESM)). Second, the RGO-CMCS-Hemin solution was successfully obtained by adding 15 mL CMCS solution to the RGO-Hemin solution and activating it with EDC/NHS at a concentration of 10 mmol/L. The RGO-CMCS-Hemin solution was successfully prepared. Finally, the RGO-CMCS-Hemin solution was poured 10 mL into a beaker, and 2 mL of 20 mM Na_2PtCl_6 and Na_2PdCl_6 solution was added, followed by 5.0 µL of hydrazine hydrate, and stirred continuously for 12 h. Then, the RGO-CMCS-Hemin/Pt@Pd NP nanozyme was successfully prepared.

Verification the peroxidase-like properties of RGO-CMCS-Hemin/Pt@Pd NP nanozyme

The peroxidase-like activity of RGO-CMCS-Hemin/Pt@Pd NP nanozyme was verified by using the TMB-H_2O_2 and OPD-H_2O_2 color development systems, respectively. Firstly, 10.0 µL 1.0 mg/mL of RGO-CMCS-Hemin/Pt@Pd NP nanozyme was added dropwise to the test tube, followed by 30.0 µL of phosphate buffer solution (PBS, 125 mmol/L, pH 5.0). Then, 10.0 µL 50 mmol/L of TMB solution and 10.0 µL 50 mmol/L of H_2O_2 solution were added respectively, stirred to make the solution homogeneous, and let the solution stand at 25℃ for 10 min to observe whether the solution turned blue. The absorbance at 652 nm of the oxidation product of TMB solution was measured using UV–vis method. Similarly, replace the TMB solution at 50 mmol/L with OPD solution at 50 mmol/L, other conditions remained unchanged, observed whether the solution turns dark yellow, and measured the absorbance of the oxidation product of OPD solution at 450 nm using UV–vis method.

Kinetics of RGO-CMCS-Hemin/Pt@Pd NP nanozyme

The steady-state kinetic studies were accomplished by keeping the concentration of one substrate constant and increasing the concentration of only one other zymolyte. To study of the effect of TMB on the catalytic performance of RGO-CMCS-Hemin/Pt@Pd NP nanozyme, 10.0 µL 1.0 mg/mL of RGO-CMCS-Hemin/Pt@Pd NP nanozyme was added dropwise to the test tube, the concentration of H_2O_2 solution was kept 5 mmol/L, and different concentrations of TMB solution were added and reacted at 25℃ for 10 min. The catalytic performance was determined by measuring the change in absorbance at 652 nm. Similarly, to investigate the effect of H_2O_2 on the catalytic performance of RGO-CMCS-Hemin/Pt@Pd NP nanozyme, 10.0 µL 1.0 mg/mL of RGO-CMCS-Hemin/Pt@Pd NP nanozyme was added dropwise to the test tube, the concentration of TMB solution was kept 5 mmol/L, different concentrations of H_2O_2 solution were added, and the catalytic performance was determined by measuring the change in absorbance at 652 nm for 10 min at 25℃. The kinetic parameters were expressed using the following double inverse equation of the Lineweaver–Burk (Eq. 1) [23]:

$$\frac{1}{v_0}=\frac{K_m}{v_{max}}\times\left(\frac{1}{[S]}+\frac{1}{K_m}\right) \quad (1)$$

The maximum reaction velocity is v_{max}, the Mie constant is K_m, and the substrate concentration is [S]. The initial velocity is v_0, v_0 is calculated using the Beer-Lambert Law $A=\varepsilon bC$ (ε is absorbance coefficient 3.9×10^4 M^{-1} cm^{-1}, b is the path length of the quartz cuvettes (1 cm in this work), and C is the molar concentration of oxTMB).

Fabrication of RGO-CMCS-Hemin/Pt@Pd NP-Apt recognition nanoprobe

The RGO-CMCS-Hemin/Pt@Pd NP nanozyme at a concentration of 1.0 mg/mL was shaken well with a vortex stirrer at a volume ratio of 1:3 with the concentration of 5.0 µmol/L Apt and incubated overnight at 25℃. Then, the products were centrifuged and washed twice with Tris–HCl buffer solution. Finally, the products (RGO-CMCS-Hemin/Pt@Pd NP-Apt) were dispersed into 500.0 µL of Tris–HCl buffer solution for further use.

Construction of RGO-CMCS-Hemin/Pt@Pd NP-based colorimetric aptasensor for the analysis of GP73

First, 10.0 µL of capture probe (AptI) at a concentration of 3.0 µmol/L was added to the centrifuge tube. Second, add 10.0 µL of 1% BSA solution and allow to stand for 30 min. Third, 10.0 µL of GP73 standard solution with different

concentrations was added to the above solution. Fourth, 10.0 μL of RGO-CMCS-Hemin/Pt@Pd NP-Apt recognition nanoprobe was added and reacted for 2 h at 25℃. Finally, a total of 10.0 μL of 8 mmol/L TMB as a color development reagent (final concentration of the system was 0.4 mmol/L) and 10.0 μL of 48 mmol/L H_2O_2 (final concentration of the system was 2.4 mmol/L) were added. The mixed solutions were reacted at 25℃ for 10 min, and then the absorbance curves at λmax = 652 nm were recorded by UV–vis spectrometry. All experiments were performed in triplicate to ensure reproducibility and reliability.

Detection of GP73 in real human serum samples

To validate the practical application of the manufactured GP73 colorimetric aptasensor, human serum samples were collected and analyzed after obtaining approval from the Ethics Committee of Guangxi Key Laboratory of Metabolic Disease Research in the 924th Hospital of Chinese People's Liberation Army Joint Logistic Support Force (Guilin, China). Two human serum samples from the healthy volunteers are selected as the analytes, in which the measured AFP concentrations are 3.12 ng/mL and 7.37 ng/mL, respectively). Different GP73 quantities were spiked into a human serum sample (volume ratio, 1:1) to obtain final concentrations of 50.0 ng/mL, 80.0 ng/mL, and 100.0 ng/mL and sonicated homogeneity. The test samples for GP73 detection were performed by the same procedures as in the case of standard samples under optimal conditions. The recovery rate for each GP73 concentration was calculated as the ratio of the result obtained via the proposed method to the corresponding spiked GP73 concentration [23]. All experiments were performed in triplicate to ensure reproducibility and reliability.

Results and discussion

The principle of the RGO-CMCS-Hemin/Pt@Pd NP-based colorimetric sensor

The schematic principle diagram of the RGO-CMCS-Hemin/Pt@Pd NP-based colorimetric sensor is shown in Fig. 1A. Firstly, RGO-CMCS-Hemin nanozyme with great peroxidase catalytic properties and huge specific surface area were synthesized by taking advantage of the large specific surface area of RGO, the huge film-forming property of CMCS, and the peroxidase property of Hemin and Pt@Pd NPs. Next, the RGO-CMCS-Hemin/Pt@Pd NP-Apt recognition nanoprobe was fabricated by binding aminated GP73 aptamer (Apt) to

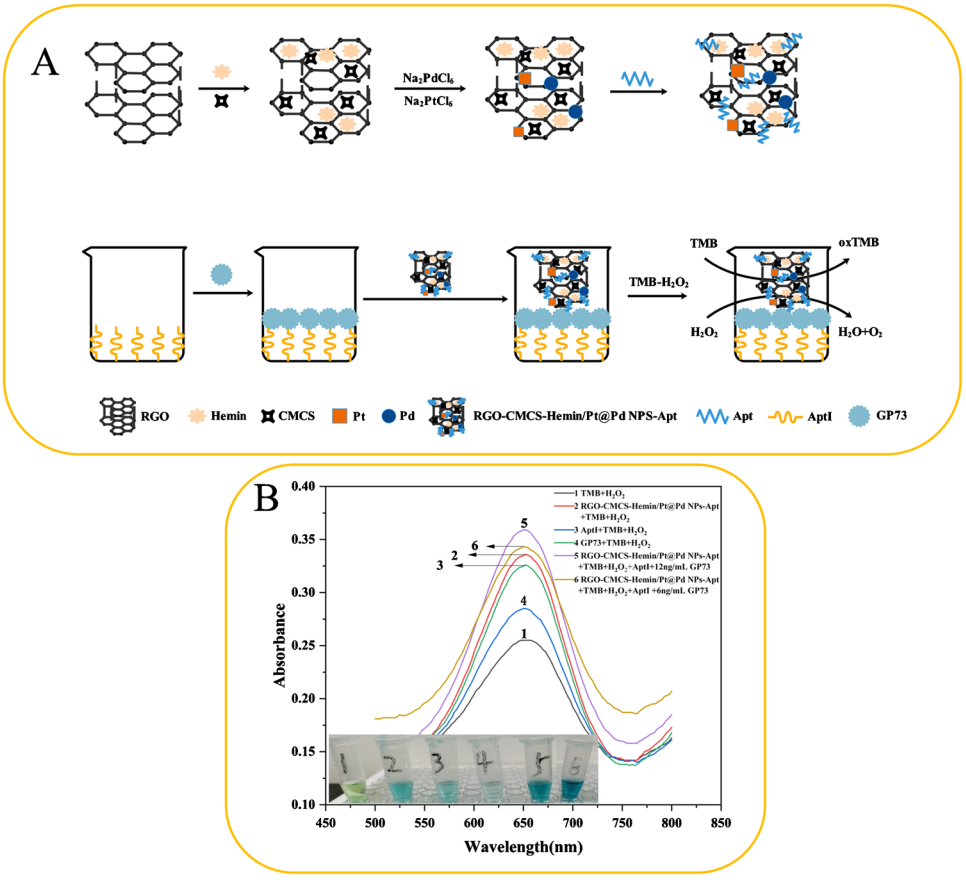

Fig. 1 **A** Schematic principle of the colorimetric biosensor based on RGO-CMCS-Hemin/Pt@Pd NPs for visual detection of GP73. **B** Validation of the colorimetric aptasensor, (1) TMB + H_2O_2, (2) RGO-CMCS-Hemin/Pt@Pd NPs-Apt+TMB + H_2O_2, (3) AptI + TMB + H_2O_2, (4) GP73 + TMB + H_2O_2, (5) RGO-CMCS-Hemin/Pt@Pd NPs + TMB + H_2O_2 + 12.0 ng/mL GP73+AptI, (6) RGO-CMCS-Hemin/Pt@Pd NPs + TMB + H_2O_2 + 6.0 ng/mL GP73+AptI

the surface of RGO-CMCS-Hemin/Pt@Pd NP nanozyme according to the electrostatic adsorption as well as the coordination bond formed by Pt@Pd and -NH_2. And the AptI was taken as a capture probe. While the targeting marker GP73 was involved, the capture probe and the recognition probe bond specifically to GP73, forming an RGO-CMCS-Hemin/Pt@Pd NP-Apt/GP73/AptI sandwich-type structure. Finally, the sandwich-type structure with good peroxidase properties mixed into TMB + H_2O_2 systems, and it catalyzed the decomposition of H_2O_2 into H_2O and O_2, which oxidized TMB to oxTMB, leading to the solution from colorless to dark blue. When the GP73 concentration increased, the capture probe could bind more GP73 and more recognition probes, forming more RGO-CMCS-Hemin/Pt@Pd NP-Apt/GP73/AptI sandwich-type structure, further enhancing its peroxidase-like activity; therefore, the solution showed a deepening blue color. The absorbance peak at 652 nm was found to increase with the increasing GP73 concentration. The colorimetric sensor has an acceptable specificity, low cost, and good visualization and can be manufactured in large quantities.

Validation of the colorimetric aptasensor

The feasibility of the proposed method was confirmed by analyzing the spectral responses of RGO-CMCS-Hemin/Pt@Pd NP nanozyme and GP73 aptamer with the TMB + H_2O_2 reporting color system. As illustrated in Fig. 1B, tube 1(TMB + H_2O_2) showed a light green color, and tube 3 (AptI + TMB + H_2O_2) and 4 (GP73 + TMB + H_2O_2) were light blue (inset of Fig. 1B); therefore, UV curves 1, 3, and 4 showed lower peak at 652 nm. For reason that TMB was oxidized partially by the oxygen in the air. Compared to tube 1, tube 2 (RGO-CMCS-Hemin/Pt@Pd NPs + TMB + H_2O_2) showed blue color (inset of Fig. 1B), and curve 2 had a medium peak at 652 nm. This was due to the peroxidase-like activity of RGO-CMCS-Hemin/Pt@Pd NP nanozyme. Compared to tube 2, tube 5 (RGO-CMCS-Hemin/Pt@Pd NPs + TMB + H_2O_2 + AptI + 12.0 ng/mL GP73) and tube 6 (RGO-CMCS-Hemin/Pt@Pd NPs + TMB + H_2O_2 + AptI + 6.0 ng/mL GP73) shows deeper blue (inset of Fig. 1B), at the same time, curves 5 and 6 showed different absorbance peaks at 652 nm. This is due to the forming a sandwich structure with more catalytic ability, which oxidizes the substrate TMB in the presence of H_2O_2 and thus changes the solution color, resulting in an increase in absorbance. As the concentration of GP73 increased (curve 5), more sandwich structures were formed, and more RGO-CMCS-Hemin/Pt@Pd NP nanozyme were involved in catalyzing H_2O_2, which in turn led to an increased oxidation of the substrate TMB and therefore a more pronounced color changed and an increase in absorbance. Thus, the absorbance was positively correlated with GP73 concentration. Therefore, RGO-CMCS-Hemin/Pt@Pd NP nanozymes are also feasible for sensor applications.

Characterization of the RGO-CMCS-Hemin/Pt@Pd NP nanozyme

Figure S1A is a typical SEM image of RGO-Hemin. Since the structure of RGO is a pleated membrane, the pleats are more evident after the introduction of Hemin. There is more membrane structure in Fig. S1B of RGO-CMCS-Hemin, which is more pronounced by adding CMCS. Figure 2A is the SEM image of RGO-CMCS-Hemin/Pt@Pd NP nanozyme; it can be seen that there are white particles in the figure, which are Pt and Pd nanoparticles formed by reduction wrapped around the surface of the material [15]. This indicates that the RGO-CMCS-Hemin/Pt@Pd NP nanozyme was prepared successfully.

Figure 2B shows the TEM picture of RGO-CMCS-Hemin/Pt@Pd NP nanozyme, and RGO-Hemin can be seen to have folding membrane-like structure, as seen in Fig. S1C. Due to the membrane-forming property of CMCS, a muslin structure of RGO-CMCS-Hemin can be seen in Fig. S1D. As seen from Fig. 2B, there are many black dots on the lamellar structure, which is the reduced formation of Pt and Pd nanoparticles, indicating the successful preparation of the material.

The X-ray diffraction spectroscopy of RGO-CMCS-Hemin/Pt@Pd NPs is shown in Fig. 2C. There are diffraction peaks at 2θ = 39.76°,46.24°, 67.45°, and 81.29º, which corresponds to the Pt Pd (111), Pt Pd (200), Pt Pd (220), and Pt Pd (311) crystal surfaces, respectively [13, 15]. All these peaks are agreement with the JCPDS standard cards of Pt (No.04–0802) and Pd (No.46–1043), which demonstrated that the metals Pt ions and Pd ions have been successfully reduced to Pt NPs and Pd NPs. The diffraction peaks at 2θ = 22.77° is the typical diffraction peak of C (120) in the RGO-CMCS-Hemin. All these results indicated that the RGO-CMCS-Hemin/Pt@Pd NP nanozyme was successfully prepared.

Figure 2D is a Raman spectrum of the RGO-CMCS-Hemin/Pt@Pd NPs, where the characteristic absorption peak in band D is 1358 cm^{-1} and the G band is 1588 cm^{-1}. Here, we choose $y = 20$ as the base line. Curve a is the RGO-Hemin with its Id/Ig of 0.820, and curve b is the RGO-CMCS-Hemin with its Id/Ig of 0.888. The increase in the Id/Ig ratio indicates that the CMCS was successfully composited on the RGO-Hemin. Compared to curve b, the RGO-CMCS-Hemin/Pt@Pd NPs in curve c has its Id/Ig of 0.947, indicating metal nanoparticles successful binding. Moreover, we found that D and G bands of RGO-Hemin and RGO-CMCS-Hemin were not completely separated. This is because the RGO in RGO-Hemin and RGO-CMCS-Hemin contain more amorphous carbon. The resulting graphene-based material

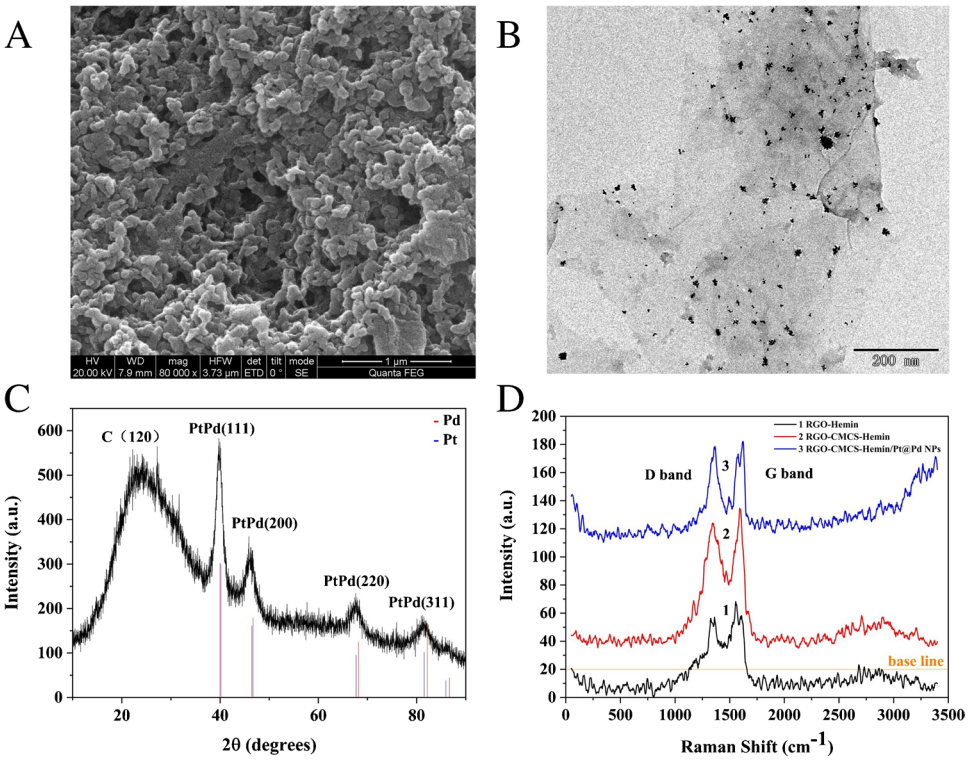

Fig. 2 **A** SEM characterization of RGO-CMCS-Hemin/Pt@Pd NPs. **B** TEM characterization of RGO-CMCS-Hemin/Pt@Pd NPs. **C** XRD characterization of RGO-CMCS-Hemin/Pt@Pd NPs. **D** Raman spectrum of RGO-Hemin (curve 1), RGO-CMCS-Hemin (curve 2), RGO-CMCS-Hemin/Pt@Pd NPs (curve 3)

contains amorphous carbon, which will lead to a poor separation of the D peak from the G peak in the resulting Raman spectrum [24, 25].

The peroxidase-like performance analysis of RGO-CMCS-Hemin/Pt@Pd NP nanozyme

After the successful preparation of RGO-CMCS-Hemin/Pt@Pd NP nanozyme, we conducted an in-depth study on the catalytic activities of the nanozyme, and the colorless H_2O_2 and TMB can also be taken as an excellent chromogenic substrate, as is shown from Fig. 3A. No adsorption peak is observed for the TMB (curve 1), H_2O_2 (curve 2), TMB + H_2O_2 solution (curve 3), and RGO-CMCS-Hemin/Pt@Pd NP nanozyme + H_2O_2 (curve 5); tubes 1, 2, 3, and 5 are almost colorless (inset of Fig. 3A), indicating the absence of an oxidation reaction. A faint adsorption peak is observed for the RGO-CMCS-Hemin/Pt@Pd NP nanozyme + TMB solution (curve 4), and tube 4 is light blue (inset of Fig. 3A); this is due to the weak oxidizing

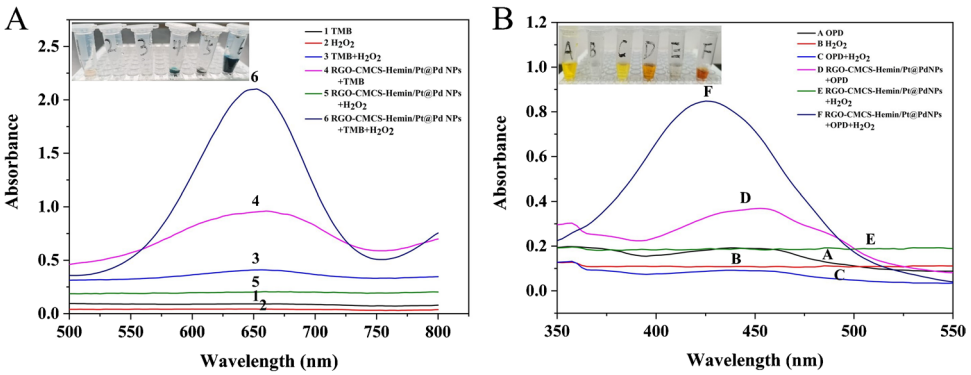

Fig. 3 **A** Peroxidase mimic activity of the RGO-CMCS-Hemin/Pt@Pd NPs in TMB-H_2O_2 reporting system, (curve 1) TMB, (curve 2) H_2O_2, (curve 3) TMB + H_2O_2, (curve 4) RGO-CMCS-Hemin/Pt@Pd NPs + TMB, (curve 5) RGO-CMCS-Hemin/Pt@Pd NPs + H_2O_2, (curve 6) RGO-CMCS-Hemin/Pt@Pd NPs + TMB + H_2O_2. **B** Peroxidase mimic activity of the RGO-CMCS-Hemin/Pt@Pd NPs in OPD-H_2O_2 reporting system, (curve 1) OPD, (curve 2) H_2O_2, (curve 3) OPD + H_2O_2, (curve 4) RGO-CMCS-Hemin/Pd@Pt NPs + OPD, (curve 5) RGO-CMCS-Hemin/Pd@Pt NPs + H_2O_2, (curve 6) RGO-CMCS-Hemin/Pd@Pt NPs + OPD + H_2O_2

property of the nanozyme that allows the slight oxidation of TMB. A strong absorption peak is observed for the RGO-CMCS-Hemin/Pt@Pd NP nanozyme + TMB + H_2O_2 solution (curve 6); tube 6 is deep blue (inset of Fig. 3A). This indicates the successful preparation of RGO-CMCS-Hemin/Pt@Pd NP nanozyme has efficient peroxidase-like catalytic activity.

Meanwhile, the colorless H_2O_2 and OPD can also be taken as an excellent chromogenic substrate, as shown in Fig. 3B. No adsorption peak is observed for the OPD (curve A), H_2O_2 (curve B), OPD + H_2O_2 (curve C), and RGO-CMCS-Hemin/Pt@Pd NP nanozyme + H_2O_2 (curve E); tubes A, B, C, and E are almost colorless or light yellow (inset of Fig. 3B), indicating the absence of an oxidation reaction. A faint adsorption peak is observed for the RGO-CMCS-Hemin/Pt@Pd NP nanozyme + OPD (curve D); tube D is light orange (inset of Fig. 3B). This is due to the weak oxidizing property of the nanozyme that allows the slight oxidation of OPD without H_2O_2. However, a strong adsorption peak is observed for the RGO-CMCS-Hemin/Pt@Pd NP nanozyme + OPD + H_2O_2 (curve F); tube F is deep orange (inset of Fig. 3B), which indicates that RGO-CMCS-Hemin/Pt@Pd NP nanozyme exist higher peroxidase-like activity for oxidation of OPD in the presence of H_2O_2.

Calculation kinetics parameter of RGO-CMCS-Hemin/Pt@Pd NP nanozyme

Figure 4A shows the experimental phenomenon and UV absorption spectrum of RGO-CMCS-Hemin/Pt@Pd NP nanozyme for different TMB concentrations in the presence of H_2O_2. The TMB concentrations in tubes A ~ G were set to 5.0–60.0 mmol/L. With increasing the TMB concentration, the system solution color becomes darker gradually (inset of Fig. 4A) and the absorption peak at 652 nm increase. This is because that the RGO-CMCS-Hemin/Pt@Pd NP nanozyme has catalytically active as a peroxidase-like enzyme and catalyzes the oxidation of TMB to oxTMB in the presence of H_2O_2. The double inverse curve of TMB is shown in Fig. 4B, and the kinetic parameters (V_{max}, K_m) were calculated using the Michaelis–Menten equation for TMB. V_{max} is calculated to be 0.106×10^{-7} Ms^{-1}, and K_m is 0.532 mM. As is well recognized that the K_m value symbolizes the affinity of the enzyme for the substrate, and the lower the K_m value, the

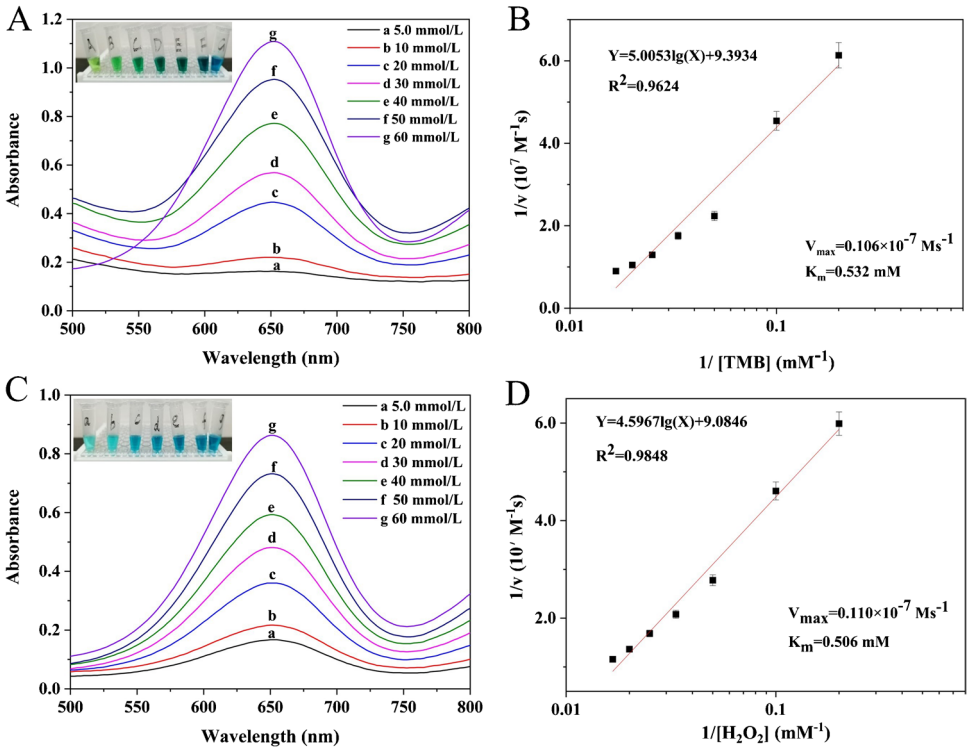

Fig. 4 **A** The steady-state kinetic studies of the RGO-CMCS-Hemin/Pt@Pd NPs nanozyme, (curve a) 5.0 mmol/L TMB, (curve b) 10.0 mmol/L TMB, (curve c) 20.0 mmol/L TMB, (curve d) 30.0 mmol/L TMB, (curve e) 40.0 mmol/L TMB, (curve f) 50.0 mmol/L TMB, (curve g) 60.0 mmol/L TMB. **B** The double inverse working curve of TMB. **C** The steady-state kinetic studies of the RGO-CMCS-Hemin/Pt@Pd NPs nanozyme, (curve a) 5.0 mmol/L H_2O_2, (curve b) 10.0 mmol/L H_2O_2, (curve c) 20.0 mmol/L H_2O_2, (curve d) 30.0 mmol/L H_2O_2, (curve e) 40.0 mmol/L H_2O_2, (curve f) 50.0 mmol/L H_2O_2, (curve g) 60.0 mmol/L H_2O_2. **D** The double inverse working curve of H_2O_2. All the above values are expressed as the median of three independent experimental analyses; the error bar represents the relative standard deviation from three independent measurements

stronger the affinity of the catalyst for the substrate. Compared with the K_m of horse radish peroxidase (HRP) for TMB ($K_m = 0.52$ mM) [23], the difference was small, indicating that the affinity of RGO-CMCS-Hemin/Pt@Pd NP nanozyme for TMB was comparable to that of HRP.

Figure 4C shows the experimental phenomenon and UV absorption spectrum of RGO-CMCS-Hemin/Pt@Pd NP nanozyme for the different H_2O_2 concentrations in the presence of TMB. The graph shows that the solution color gradually darkens as the H_2O_2 concentration increased (inset of Fig. 4C). By measuring the peak absorption at 652 nm for comparison, the absorbance increases with increasing H_2O_2 concentration in the range of 5.0 ~ 60 mmol/L. The double inverse curve of H_2O_2 can be seen in Fig. 4D; we calculated V_{max} to be 0.106×10^{-7} Ms^{-1} and K_m to be 0.532 mM according to the Michaelis–Menten equation. Compared with the K_m of horse radish peroxidase (HRP) for H_2O_2 ($K_m = 18.48$ mM) [23], the K_m values of RGO-CMCS-Hemin/Pt@Pd NP nanozyme were lower than that of HRP, demonstrating that the RGO-CMCS-Hemin/Pt@Pd NP nanozyme has superior affinity for H_2O_2 substrates, more than 73 times that of HRP.

In addition, the peroxidase-like kinetic parameters of the RGO-CMCS-Hemin/Pt@Pd NP nanozyme are compared with other nanozymes and listed in Table 1. Kinetic analysis showed that the Km for TMB of RGO-CMCS-Hemin/Pt@Pd NPs ($K_m = 0.532$) is lower than Fe_2Ni-MOF ($K_m = 0.5567$), γ-Fe_2O_3 NPs ($K_m = 1.24$), and RIgG@Cu-MOF ($K_m = 3.91$), but higher than CDs/PBNPs ($K_m = 0.311$) and FeCo-ONSs/heparin ($K_m = 0.26$). This indicates that the affinity of RGO-CMCS-Hemin/Pt@Pd NPs nanozyme for the substrate TMB is relatively average, and a slightly higher concentration of TMB may be required as a substrate for GP73 detection in practical applications. In terms of affinity with H_2O_2, RGO-CMCS-Hemin/Pt@Pd NPs ($K_m = 0.506$) had the lowest K_m. This indicates that RGO-CMCS-Hemin/Pt@Pd NPs has higher affinity with H_2O_2. Therefore, a relatively low concentration of H_2O_2 can make RGO-CMCS-Hemin/Pt@Pd NPs reach the maximum catalytic activity in the application.

Table 1 Comparison of the peroxidase-like kinetic parameters of the RGO-CMCS-Hemin/Pt@Pd NPs nanozyme with other nanozymes

Catalyst	Substrate	K_m(mM)	V_{max}(10^{-7} Ms^{-1})	Ref
CDs/PBNPs	TMB	0.311	0.588	[26]
	H_2O_2	3.457	0.612	
Fe_2Ni-MOF	TMB	0.5567	3.0386	[27]
	H_2O_2	0.1337	1.3504	
FeCo-ONSs/heparin	TMB	0.26	0.758	[28]
	H_2O_2	0.98	0.671	
γ-Fe_2O_3 NPs	TMB	1.24	1.301	[29]
	H_2O_2	21.54	6.671	
RIgG@Cu-MOF	TMB	3.91	5.445	[30]
	H_2O_2	7.37	1.075	
RGO-CMCS-Hemin/Pt@Pd NPs	TMB	0.532	0.106	This work
	H_2O_2	0.506	0.110	

Among RGO-CMCS-Hemin/Pt@Pd NP nanozyme, the large specific area of RGO provides a good linkage site for Hemin and CMCS, and the peroxide-like nature of RGO and Hemin provides good catalytic activity. By introducing Pt@Pd, due to the good catalytic activity and interaction of this alloy, the catalytic activity of RGO-CMCS-Hemin/Pt@Pd NP nanozyme is further improved. Therefore, the RGO-CMCS-Hemin/Pt@Pd NP nanozyme has good peroxidase-like catalytic activity.

Colorimetric aptasensor for GP73 determination

Several key parameters, including the concentrations of capture probe concentration, incubation temperature, pH, reaction time of aptamer, and GP73, were optimized to ensure the efficient performance of the proposed detection system. The results (Fig. S3 and Fig. S4) and the related description were found in ESM. Under the optimized experimental conditions (capture probe concentration of 3 μmol/L, incubation temperature of 25 ℃, pH of 4.0, aptamer, and GP73 reaction time of 120 min), different concentrations of GP73 were detected by the RGO-CMCS-Hemin/Pt@Pd NP-based colorimetric aptasensor. Figure 5A presents the experimental phenomenon and UV–vis absorption spectrum of the designed colorimetric sensor for the different GP73 concentration (0, 10.0, 30.0, 50.0, 70.0, 90.0, and 110.0 ng/mL). The system solution color deepened as the GP73 concentration increased (inset of Fig. 5A), and the absorbance at 652 nm increased with the increase of GP73 concentration. This finding confirms that as GP73 concentration increases, more and more GP73 binds to aptamers to form more aptamer-GP73-aptamer complexes, and more RGO-CMCS-Hemin/Pt@Pd NP nanozyme in the aptamer-GP73-aptamer complexes catalyzes more H_2O_2 and oxidizes more TMB to oxTMB, making the solution darker and the absorbance enhancing. According to Fig. 5B, in the range of 10.0 to 110.0 ng/mL, GP73 concentration is linearly related to the absorption intensity. The standard curve equation was $Y = 0.0032X + 0.3171$, $R^2 = 0.9906$ (where Y represented the absorption intensity at 652 nm and X indicated GP73 concentration). The formula LOD = 3S/k (S was the criterion bias of six duplicate blank signals, k was the slope of the standard curve) is used to calculate the limit of detection (LOD) [31]. By calculating, the LOD is 4.7 ng/mL.

In clinical, the concentration of GP73 in normal human serum is a few tens of nanograms per milliliter. When the

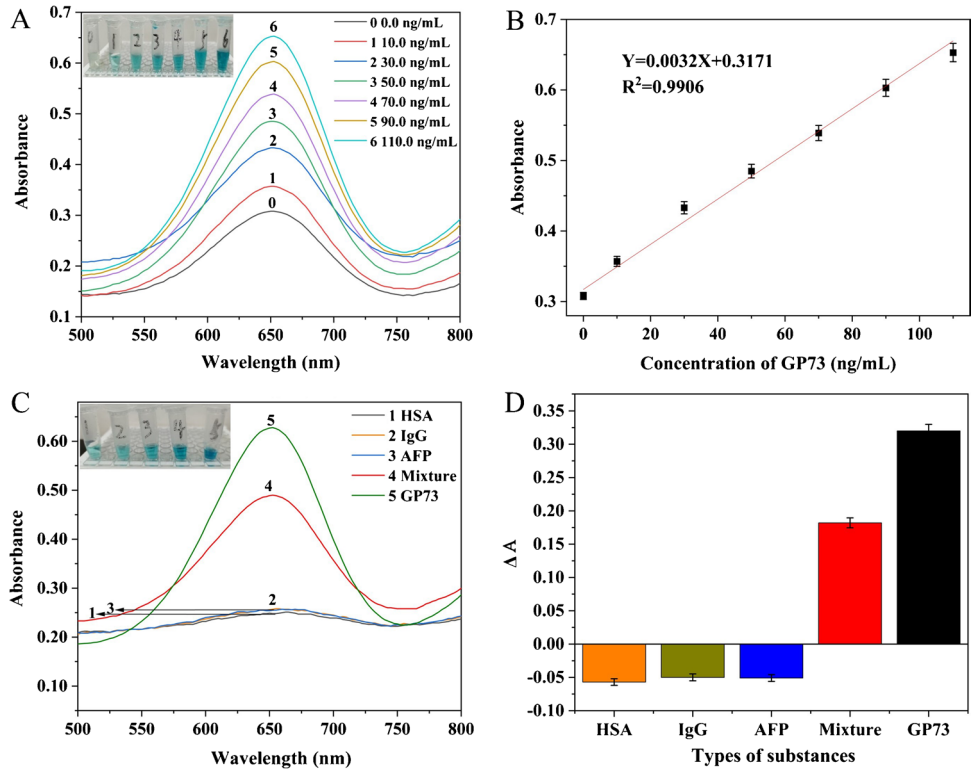

Fig. 5 **A** The absorbance of different concentrations GP73 under the optimized experimental conditions and experimental phenomenon, (0) 0 ng/mL GP73, (1) 10.0 ng/mL GP73, (2) 30.0 ng/mL GP73, (3) 50.0 ng/mL GP73, (4) 70.0 ng/mL GP73, (5) 90.0 ng/mL GP73, (6) 110.0 ng/mL GP73. **B** The calibration plots of the relationship between the absorbance intensity at 652 nm and the GP73 concentration. **C** The absorbance of different protein to verify the specificity of the GP73 colorimetric sensor, (1) 1.0 μg/mL HSA, (2) 1.0 μg/mL IgG, (3) 1.0 μg/mL AFP, (4) mixture includes HSA, IgG, AFP and GP73, (5) 100.0 ng/mL GP73. **D** Histogram of the specificity for GP73 colorimetric sensor. All the above values are expressed as the median of three independent experimental analyses; the error bar represents the relative standard deviation from three independent measurements

GP73 concentration exceeds 77.39 ng/mL, the risk of having HCC is about 92.31% [32]. Moreover, a comparison between the proposed colorimetric method and other biosensors for GP73 detection is shown in Table 2, Compared to other methods in Table 2, the sensor exhibited an extremely high level of performance in detecting low concentrations of GP73. Our designed sensors cannot reach this level. The LOD of our RGO-CMCS-Hemin/Pt@Pd NP-based colorimetric aptasensor is high, which may be owing to the following factors; the affinity between GP73 and aptamer is not powerful enough, resulting in an incomplete connection. Besides, the aptamer-GP73-aptamer sandwich complex has a spatial steric effect, which hinders the catalytic efficiency of RGO-CMCS-Hemin/Pt@Pd NP nanozyme. However, the

Table 2 Comparison the GP73 determination with other methods

Method	Linear range	LOD	Ref
Turbidimetric immunoassay	20–320 ng/mL	2.11 ng/mL	[33]
Electrochemical immunosensor	0.0003–6.0 ng/mL	0.0001 ng/mL	[34]
B-HRP/A-LCA/AuNPs electrochemistry	0.01 ~ 25 ng/mL	0.007 ng/mL	[21]
Electrochemiluminescence and immunoassay	0.015 ~ 0.7 ng/mL	0.015 ng/mL	[5]
xMAP (multi-analyte suspension array) technology	0.01 ~ 50 ng/mL	0.48 ng/mL	[35]
Immunoblotting and ELISA	0.25–4.0 ng/mL	0.25 ng/mL	[36]
Manganese modified CdTe/CdS quantum dots immunoassay	20 ~ 150 ng/mL	10.0 ng/mL	[31]
RGO-Mn_3O_4 nanozyme colorimetry	10 ~ 250 ng/mL	5.42 ng/mL	[12]
RGO-CMCS-Hemin/Pt@Pd nanozyme colorimetry	10 ~ 110 ng/mL	4.7 ng/mL	This work

linear range of our sensor is more closely matched to the clinical detection requirements. Compare with other methods, the colorimetric aptasensor is much less costly and visualizes the results. And it does not require complex and expensive instrumentation in its design and use. Thus, this low-cost colorimetric aptasensor provides a new and promising platform for the design in clinical testing.

Specificity of the GP73 colorimetric aptasensor

To verify the specificity of the GP73 colorimetric sensor, HSA, IgG, AFP, GP73, and mixed solutions were selected for comparison. The concentrations of tube 1 (HSA), tube 2 (IgG), tube 3 (AFP), and tube 5 (GP73) were set at 1.0 μg/mL, 1.0 μg/mL, 1.0 μg/mL, and 0.1 μg/mL, respectively, and tube 4 was a mixture of the above four materials, the absorbance at 652 nm for each above solution was recorded, and the experimental phenomenon and UV–vis absorption spectrum were present in Fig. 5C. The results are expressed as $\Delta A = A\text{-}A0$, where A0 indicates the absorbance value at 652 nm in the absence of the sample and A indicates the absorbance value of each sample, respectively. Figure 5D was the histogram of the specificity for GP73 colorimetric sensor. The ΔA of HSA, IgG, and AFP were − 0.057, − 0.050, and − 0.051, respectively. The concentration of GP73 is one-tenth that of the other non-specific proteins and has the highest UV–vis absorption compared to the other three substances, and its ΔA was 0.320. The mixture has the second highest ΔA at 0.182. The above results indicate that the colorimetric sensor based on RGO-CMCS-Hemin/Pt@Pd NP nanozymes has some cross-sensitivity to other non-specific proteins. This may be due to other proteins covering the GP73 binding site when the mixture was detected, resulting in insufficient amounts of GP73 binding to the aptamer and ultimately resulting in a lower absorbance for the mixture. The sensor may exhibit certain disadvantages when performing complex sample detection. However, the specificity results of the sensor are still acceptable.

Determination of GP73 in the human serum samples

In this study, two human serum samples from the healthy volunteers are selected as the analytes, in which the measured AFP concentrations are 3.12 ng/mL and 7.37 ng/mL, respectively). Different GP73 quantities were spiked into a human serum sample (volume ratio, 1:1) to obtain final concentrations of 50.0 ng/mL, 80.0 ng/mL, and 100.0 ng/mL and sonicated homogeneity. Then, the test samples were detected with the prepared colorimetric sensor through the absorbance at 652 nm, and the GP73 content in the actual samples was calculated using the GP73 standard curve ($Y = 0.0032X + 0.9906$). Each experiment was measured three times and the results were presented in Table 3. The relative standard deviation (RSD) of the GP73 colorimetric sensor based on RGO-CMCS-Hemin/

Table 3 Analysis of the GP73 test results in the actual serum samples

Actual serum	Added GP73 concentration (ng/mL)	Detection GP73 concentration (ng/mL)	Average of GP73 detection concentration (ng/mL)	RSD (%)	Recovery (%)
		52.30			
	50.0	49.94	49.94	3.75	99.9
		48.59			
		81.25			
Sample 1	80.0	79.91	79.91	1.90	99.9
		78.22			
		103.14			
	100.0	98.42	98.42	4.79	98.4
		93.71			
		51.62			
	50.0	51.29	51.29	2.49	103
		49.27			
		85.97			
Sample 2	80.0	78.56	78.56	5.44	98.2
		85.97			
		106.84			
	100.0	106.51	106.51	3.75	107
		99.77			

(Sample 1 had 3.12 ng/mL of AFP, and Sample 2 had 7.37 ng/mL of AFP)

Pt@Pd NP nanozyme was in the range of 1.90 to 5.44%, and the recoveries for GP73 via the proposed aptasensor ranged from 98.2 to 106%. The data indicated that the GP73 colorimetric sensor based on RGO-CMCS-Hemin/Pt @Pd NPs can detect GP73 content in human serum.

Conclusions

In conclusion, we have constructed a facile colorimetric aptasensor for GP73 detection based on the RGO-CMCS-Hemin/Pt@Pd NPs with peroxidase-like activity. The RGO-CMCS-Hemin/Pt@Pd NP nanozymes were successfully synthesized under mild conditions. The steady-state kinetics of RGO-CMCS-Hemin/Pt@Pd NPs for the catalytic oxidation of TMB in the presence of H_2O_2 was investigated in order to demonstrate that the RGO-CMCS-Hemin/Pt@Pd NPs has high affinity to substrates: TMB and H_2O_2. It is a key part of this sensor and plays an important role for the sensor to detect GP73. Taking advantage of the good peroxidase-like properties, RGO-CMCS-Hemin/Pt@Pd NPs can oxidase colorless TMB into blue oxTMB in the presence of H_2O_2, and the absorbance of the system at 652 nm changed consequently, which realize the sensitive colorimetric detection of GP73. The colorimetric aptasensor has a linear range that is relatively well suited for clinical detection. The sensor also has an acceptable specificity and good recovery. Although the proposed RGO-CMCS-Hemin/Pt@Pd NP-based colorimetric sensor has a relatively high LOD and some cross-sensitivity, it is still insufficient for practical clinical detection. Future work will focus on the obtaining a more rapid response time and lower LOD for the proposed RGO-CMCS-Hemin/Pt@Pd NP-based colorimetric aptasensor. This aptasensing format is expected to considerably promote the development of small portable devices for point-of-care test in the future.

Supplementary Information The online version contains supplementary material available at https://doi.org/10.1007/s00604-022-05480-6.

Author contribution Xinhao LI: Methodology, data curation, writing—original draft preparation. Shengnan LI: Software; writing, original draft preparation; validation. Qiuyan Lv: Methodology, conceptualization. Chaoxian WANG: Visualization, software, data curation. Jintao Liang: Data curation, writing—reviewing and editing. Zhide ZHOU: Supervision, writing—reviewing and editing. Guiyin LI: Supervision, writing—reviewing and editing.

Funding This work was supported by the National Nature Science Foundation of China (No. 62161009), Projects of Talents Recruitment of GDUPT (XJ2022000401), the Open Fund of Guangxi Key Laboratory of Information Materials (No. 211022-K), and the Fund of Guangxi Key laboratory of Metabolic Diseases Research (No. 20–065-76).

Declarations

Ethics approval The human serum samples used in this study were approved by the Guangxi Key Laboratory of Metabolic Diseases Research Ethics Committee in Guilin, China.

Conflict of interest The authors declare no competing interests.

References

1. Bray F, Ferlay J, Soerjomataram I, Siegel RL, Torre LA, Jemal A (2018) Global cancer statistics 2018: Globocan estimates of incidence and mortality worldwide for 36 cancers in 185 countries. CA: a Cancer J Clin 68:394–424. https://doi.org/10.3322/caac.21492
2. Kimhofer T, Fye H, Taylor-Robinson S, Thursz M, Holmes E (2015) Proteomic and metabonomic biomarkers for hepatocellular carcinoma: a comprehensive review. Brit J Cancer 112:1141–1156. https://doi.org/10.1038/bjc.2015.38
3. Wang L, Yao M, Liu S, Yang D, Wen X, Ning J, Wang L, Zhou G, Xu Q, Chen X, Zhao J, Lu F (2020) Serum golgi protein 73 as a potential biomarker for hepatic necroinflammation in population with nonalcoholic steatohepatitis. Dis Markers 2020:6036904. https://doi.org/10.1155/2020/6036904
4. Marrero JA, Romano PR, Nikolaeva O, Steel L, Mehta A, Fimmel CJ, Comunale MA, D'Amelio A, Lok AS, Block TM (2005) GP73, a resident Golgi glycoprotein, is a novel serum marker for hepatocellular carcinoma. J Hepatol 43:1007–1012. https://doi.org/10.1016/j.jhep.2005.05.028
5. Lin Y, Jia J, Yang R, Chen D, Wang J, Luo F, Guo L, Qiu B, Lin Z (2019) Ratiometric immunosensor for GP73 detection based on the ratios of electrochemiluminescence and electrochemical signal using DNA tetrahedral nanostructure as the carrier of stable reference signal. Anal Chem 91:3717–3724. https://doi.org/10.1021/acs.analchem.9b00013
6. Yang Z, Qian J, Yang X, Jiang D, Du X, Wang K, Mao H, Wang K (2015) A facile label-free colorimetric aptasensor for acetamiprid based on the peroxidase-like activity of hemin-functionalized reduced graphene oxide. Biosens Bioelectron 65:39–46. https://doi.org/10.1016/j.bios.2014.10.004
7. Shaban SM, Kim DH (2021) Recent advances in aptamer sensors. Sensors (Basel, Switzerland) 21. https://doi.org/10.3390/s21030979
8. Ruirui Z, Yunfeng B, Xiaoliang C, Feng F, Shaomin. Shuang, (2020) Advances in the study of aptamers in cancer diagnosis and targeted therapy. Chem Bulletin 83:977–985. https://doi.org/10.14159/j.cnki.0441-3776.2020.11.003
9. Yuanbin G, Kun L (2021) Advances in the study of nucleic acid aptamers in cancer diagnosis. Chem Bulletin 84:40–46. https://doi.org/10.14159/j.cnki.0441-3776.2021.01.006
10. Du J, Hong J, Xu C, Cai Y, Xiang B, Zhou C, Xu X (2015) Screening and identification of ssDNA aptamer for human GP73. Biomed Res Int 2015:610281. https://doi.org/10.1155/2015/610281
11. Xiao S, Lu J, Sun L, An S (2022) A simple and sensitive AuNPs-based colorimetric aptasensor for specific detection of azlocillin. Spectrochim Acta A 271:120924. https://doi.org/10.1016/j.saa.2022.120924
12. Chen M, Zhong L, Feng H, Li G (2021) Golgi protein 73 colorimetric biosensor based on reduced graphene oxide-trimanganese tetroxide nanozyme. J Phys Conf Ser 2021.https://doi.org/10.1088/1742-6596/2021/1/012065

13. Watanabe T, Hiraoka Y, Suda K, Kawamoto T, Yano H, Inukai J, Hirosawa I (2019) Development of combined small-angle X-ray scattering and fluorescence yield X-ray absorption spectroscopy measurement systems for characterization of structural and chemical information of Pt alloy nanoparticle catalyst. ECS MA 2019–02:1593–1593. https://doi.org/10.1149/ma2019-02/35/1593
14. DeRita L, Resasco J, Dai S, Boubnov A, Thang HV, Hoffman AS, Ro I, Graham GW, Bare SR, Pacchioni G, Pan X, Christopher P (2019) Structural evolution of atomically dispersed Pt catalysts dictates reactivity. Nat Mater 18:746–751. https://doi.org/10.1038/s41563-019-0349-9
15. Qu Y, Zheng Z, Yu Z, Song M, Zhang Y, Zhao Y, Yu J (2021) Chain-like PtPd nanoparticles with a long-time stability as an efficient electrocatalyst for alcohols oxidation reaction. Colloid Surface A 631:127756. https://doi.org/10.1016/j.colsurfa.2021.127756
16. Ji X, Han Z, Li J, Deng Y, Han X, Zhao J, Zhao X, Chen C (2019) MoSx co-catalytic activation of H(2)O(2) by heterogeneous hemin catalyst under visible light irradiation. J Colloid Interf sci 557:301–310. https://doi.org/10.1016/j.jcis.2019.09.027
17. Kolupaev YE, Shkliarevskyi MA, Karpets YV, Shvidenko NV, Lugovaya AA (2021) ROS-dependent induction of antioxidant system and heat resistance of wheat seedlings by hemin. Russ J Plant Physl 68:322–330. https://doi.org/10.1134/S102144372101009X
18. Lei L, Tu Q, Jiao L, Xiang S, Wang L, Ran X, Xiao B, Feng G, Feng J, Zhang C (2022) Reactive oxygen species scavenging by hemin-based nanosheets reduces Parkinson's disease symptoms in an animal model. Chem Eng J 432.https://doi.org/10.1016/j.cej.2021.134356
19. Zhang G, Liu Z, Fan L, Guo Y (2018) Electrochemical prostate specific antigen aptasensor based on hemin functionalized graphene-conjugated palladium nanocomposites. Microchim Acta 185:159. https://doi.org/10.1007/s00604-018-2686-9
20. Li J, Zhuang S (2020) Antibacterial activity of chitosan and its derivatives and their interaction mechanism with bacteria: current state and perspectives. Eur Polym J 138.https://doi.org/10.1016/j.eurpolymj.2020.109984
21. Li J, Wang B, Gu S, Yang Y, Wang Z, Xiang Y (2017) Amperometric low potential aptasensor for the fucosylated Golgi protein 73, a marker for hepatocellular carcinoma. Microchim Acta 184:3131–3136. https://doi.org/10.1007/s00604-017-2334-9
22. Li G, Feng H, Shi X, Chen M, Liang J, Zhou Z (2021) Highly sensitive electrochemical aptasensor for glypican-3 based on reduced graphene oxide-hemin nanocomposites modified on screen-printed electrode surface. Bioelectrochemistry 138:107696. https://doi.org/10.1016/j.bioelechem.2020.107696
23. Wang L, Zhou H, Wu X, Song Y, Huang Y, Yang X, Chen X (2022) A novel colorimetric aptasensor for sensitive tetracycline detection based on the peroxidase-like activity of Fe_3O_4@Cu nanoparticles and "sandwich" oligonucleotide hybridization. Microchim Acta 189. https://doi.org/10.1007/s00604-022-05195-8
24. Han X, Russo PA, Triolo C, Santangelo S, Goubard-Bretesché N, Pinna N (2020) Comparing the performance of Nb_2O_5 composites with reduced graphene oxide and amorphous carbon in Li- and Na-Ion electrochemical storage devices. ChemElectroChem 7:1689–1698. https://doi.org/10.1002/celc.202000181
25. Hui W, Tao P, Zongkui K, Jian Z, Kun C, Daping H, Mu P, Shichun M (2015) Core-shell graphene@amorphous carbon composites supported platinum catalysts for oxygen reduction reaction. Chinese J Catal 36:490–495. https://doi.org/10.1016/S1872-2067(14)60211-4
26. Song Y, Liu W, Mu X, Zhong X, Cui A, Sun Y, Crockett JR, Bao Y, Shan G, Chen Y (2021) Photothermal-enhanced peroxidase-like activity of CDs/PBNPs for the detection of Fe(3+) and cholesterol in serum samples. Microchim acta 189:30. https://doi.org/10.1007/s00604-021-05129-w
27. Mu Z, Wu S, Guo J, Zhao M, Wang Y (2022) Dual mechanism enhanced peroxidase-like activity of iron–nickel bimetal–organic framework nanozyme and its application for biosensing. ACS Sustain Chem Eng 10:2984–2993. https://doi.org/10.1021/acssuschemeng.1c07975
28. Zhou C, Chen J, Wang G, Su X (2022) Heparin-enhanced peroxidase-like activity of iron-cobalt oxide nanosheets for sensitive colorimetric detection of trypsin. Microchim Acta 189:135. https://doi.org/10.1007/s00604-022-05227-3
29. Wang X, Ouyang F, Cui L, Xiong T, Guan X, Guo Y, Duan S (2019) Surface coating–modulated peroxidase-like activity of maghemite nanoparticles for a chromogenic analysis of cholesterol. J Nanopart Res 21.https://doi.org/10.1007/s11051-019-4662-7
30. Wang C, Gao J, Tan H (2018) Integrated antibody with catalytic metal-organic framework for colorimetric immunoassay. ACS Appl Mater Interfaces 10:25113–25120. https://doi.org/10.1021/acsami.8b07225
31. Liu W, Zhang A, Xu G, Wei F, Yang J, Hu Q (2016) Manganese modified CdTe/CdS quantum dots as an immunoassay biosensor for the detection of Golgi protein-73. J Pharmaceut Biomed 117.https://doi.org/10.1016/j.jpba.2015.08.020
32. Jing J, Ye W, Jiang Y, Ma J, Zhu M, Ma J, Zhou H, Yu L, Yang Y, Wang SC (2017) The value of GPC3 and GP73 in clinical diagnosis of hepatocellular carcinoma. Clin Lab 63:1903–1909. https://doi.org/10.7754/Clin.Lab.2017.170712
33. Xia Y, Yao H, Xu P, Xu C, Sun L, Zhu F, Li Y (2017) Comparison of two latex nanoparticles with different diameters and the application in detection of biomarker Golgi protein 73 in hepatocellular carcinoma. Nanosci Nanotech Let 9:398–405. https://doi.org/10.1166/nnl.2017.2354
34. Zhang Y, Huang X, Luo F, Lei Y, Chen L, Weng Z, Guo L, Lin Z (2018) Highly sensitive electrochemical immunosensor for Golgi protein 73 based on proximity ligation assay and enzyme-powered recycling amplification. Anal Chim Acta 1040:150–157. https://doi.org/10.1016/j.aca.2018.08.021
35. Wu Y, Ma J, Wang Y, Zhang Y, Hou Y, Zhang C, Sun H, Sun J, Wang Z, Li N (2018) Development of an alpha-fetoprotein and Golgi protein 73 multiplex detection assay using xMAP technology. Clin Chim Acta 482:209–214. https://doi.org/10.1016/j.cca.2018.03.039
36. Aixia Z, Brian C (2012) Generation and characterization of an anti-GP73 monoclonal antibody for immunoblotting and sandwich ELISA. J Biom Res 26.https://doi.org/10.7555/JBR.26.20120057

Authors and Affiliations

Xinhao Li[1] · Shengnan Li[1] · Qiuyan Lv[1] · Chaoxian Wang[2] · Jintao Liang[1] · Zhide Zhou[1] · Guiyin Li[1,2]

[1] School of Life and Environmental Sciences, Guangxi Key Laboratory of Information Materials, Guilin University of Electronic Technology, Guilin, Guangxi 541004, People's Republic of China

[2] College of Chemistry, Guangdong University of Petrochemical Technology, Guandu Road, Maoming, Guangdong 525000, People's Republic of China